

1 Processes Regulating Short Lived Species in the
2 Tropical Tropopause Layer

A. Gettelman, P. Lauritzen, M. Park, J. E. Kay¹

3 National Center for Atmospheric Research

Submitted to JGR: 22 January 2009, Revised : 29 March 2009

¹also at: Department of Atmospheric
Science, Colorado State University, Fort
Collins, Colorado, USA.

Copyright 2009 by the American Geophysical Union.

0148-0227/09/\$9.00

Abstract.

A one dimensional model of vertical transport in the tropical tropopause layer (TTL) is developed. The model uses vertical advection, a convective source and a chemical sink to simulate the profiles of very short lived substances (VSLS) in the TTL. The model simulates evanescent profiles of short lived hydrocarbon species observed by satellite, and is also used to simulate short lived bromine species. Tracers with chemical lifetimes of 25 days or longer have significant concentrations in the stratosphere and vertical advection is critical. Convection is important up to its peak altitude, nearly 19km. Convection dominates the distribution of species with lifetimes less than 25 days. The annual cycle of species with lifetimes longer than 25 days is governed primarily by the variations of vertical velocity, not convection. This is particularly true for carbon monoxide, where a seasonal cycle in the lower stratosphere of the right phase is produced without variations in tropospheric emissions. An analysis of critical short lived bromine species (CH_2Br_2 and CHBr_3) indicates that substantial amounts of these tracers may get advected into the lower stratosphere as source gases at 18km, and are estimated to contribute 2.8 pptv (1.1–4.1) to stratospheric bromine.

1. Introduction

4 Transport in the region around the tropical tropopause, the Tropical Tropopause Layer
5 (TTL) is important for setting the chemical boundary conditions of the stratosphere. This
6 is particularly true for species with lifetimes $< \sim 2$ months, whose chemical or removal life-
7 time is comparable to or shorter than the transit time through the TTL, estimated at ~ 60
8 days [Fueglistaler *et al.*, 2004]. One important example are bromine compounds, which
9 can turn bromine into active forms that can efficiently deplete ozone in the stratosphere.
10 Currently there are large uncertainties of the reactive bromine in the lower stratosphere
11 [Salawitch *et al.*, 2005; World Meteorological Organization, 2007]. Uncertainty is driven
12 by sources, as well as how very short lived substances (VSLs: defined here as lifetimes
13 < 6 months) enter the stratosphere through the TTL. There is also uncertainty in how
14 dehydration and wet removal occurs [Sinnhuber and Folkins, 2006].

15 Transport in the TTL occurs through rapid vertical motion in deep convection and slow
16 vertical transport outside of clouds. The TTL transit time for each pathway may be very
17 different, and the impact on trace species may be very different [Fueglistaler *et al.*, 2008].
18 Transit may vary in space and time, with some regions such as the boreal summer Asian
19 Monsoon contributing disproportionately [Gettelman *et al.*, 2004b]. Washout of chemical
20 species may also be important [Sinnhuber and Folkins, 2006].

21 In this work we develop a model of the TTL that simulates the effect of key processes on
22 chemical constituents in order to better understand the balance of processes responsible
23 for TTL transport. The model is similar to those developed by Read *et al.* [2004] to
24 examine water vapor dehydration in the TTL and Sinnhuber and Folkins [2006] to explore
25 bromoform (CHBr_3) in the stratosphere.

26 The model is an idealized model of mean tropical transport that simulates tracers with
27 various lifetimes, and compares the resulting profiles to satellite observations. We will
28 focus on the effect of convective transport, large scale vertical motions and chemical
29 production or loss in the region. Our goal is to determine the range of tracer lifetimes
30 that result in significant stratospheric injection, and for key bromine containing species,
31 quantify how much bromine they may carry into the stratosphere. Section 2 contains a
32 description of the methodology, section 3 describes the model, section 4 contains results,
33 and conclusions are in section 5.

2. Methodology and observations

2.1. Observations for comparison

34 Observations from the Atmospheric Chemistry Experiment (ACE) Fourier Transform
35 Spectrometer (FTS) provide information on short-lived species in the TTL. ACE-FTS is
36 a limb-viewing Fourier Transform Spectrometer [*Bernath et al.*, 2005]. ACE is in an orbit
37 designed to maximize observations at high-latitudes, but limited information is available
38 for the tropics. Retrievals of species with different lifetimes from ACE surrounding the
39 Asian Monsoon for the data used here representing 2004–2006 were presented by *Park*
40 *et al.* [2008].

41 Figure 1 shows ACE profiles of 3 tracers with very different lifetimes. Data represent
42 130–220 profiles in each season between 20°S–20°N latitude from 2004–2006. Carbon
43 monoxide (CO) has a lifetime of ~ 60 days. Ethane (C₂H₆) has a lifetime of ~ 45 days and
44 acetylene (C₂H₂) has a lifetime of ~ 15 days. Tracers fall off rapidly with height above 12–
45 15 km, higher for species with longer lifetimes. Seasonally, there are higher tropospheric
46 concentrations of all three tracers in September–November (SON) in the troposphere, and

47 higher concentrations of CO and C₂H₆ in the TTL (16–20km). Table 1 shows the annual
48 average fraction of tracer remaining at various altitudes from Figure 1. The shorter lived
49 species have a lower fraction of their tropospheric mixing ratio remaining at any altitude,
50 and this decreases rapidly above the tropopause.

51 ACE observations of these hydrocarbons represent a range of lifetimes. We also run
52 the model with tracers more representative of short lived bromine and iodine containing
53 species that might affect stratospheric ozone: Dibromomethane (CH₂Br₂) with a lifetime
54 of 120 days, bromoform (CHBr₃) with a lifetime of 26 days and methyl iodide (CH₃I) with
55 a lifetime of 6 days [*World Meteorological Organization*, 2007]. We do not have satellite
56 observations of these species in the TTL for comparison with simulations.

2.2. Why a 1D model?

57 Three dimensional motions (3D) are critical for understanding the complex motions and
58 interactions between convective and large scale processes in the TTL. There have been
59 many studies analyzing processes in the TTL using 3D trajectory based models [*Gettelman*
60 *et al.*, 2002a; *Fueglistaler and Haynes*, 2005] or complex coupled chemistry-climate models
61 [*Gettelman and Birner*, 2007]. However, there still is utility in using simple column models
62 to try to understand processes, such as those explored by *Sherwood and Dessler* [2001].
63 Simple models allow complex processes to be reduced to a few simple relationships, and
64 allow results to be directly related to individual terms or processes. They also allow rapid
65 sensitivity testing of the parameter space of simulated processes. Results can be designed
66 to compare to observations at similar scales. It is in this spirit that we develop and present
67 a one dimensional (1D) vertical transport model for short lived species in the TTL.

68 The model is similar to previous 1D and 2D models of the TTL. *Sinnhuber and Folkins*
 69 [2006] used the TTL convective detrainment model of *Folkins and Martin* [2005] to in-
 70 vestigate how bromoform is transported in the TTL, and found significant transport of
 71 bromine into the stratosphere occurred, and it was dependent on the assumed washout
 72 rate for bromine. *Read et al.* [2004] and *Read et al.* [2008] used a version of the model
 73 originally developed by *Holton and Gettelman* [2001] and *Gettelman et al.* [2002a] to look
 74 at transport of tracers such as water vapor and carbon monoxide seasonally in the TTL.
 75 Here we develop a 1D model to explore a variety of short lived species and look at the
 76 transport times into the stratosphere.

3. Model Description

77 This section describes the basic formulation of the 1D transport model and the inputs
 78 used to drive the model.

3.1. Transport

The model is constructed as a one dimensional transport model, with a basic tendency equation for each tracer:

$$\frac{\partial[X_i]}{\partial t} = \frac{\partial[X_i]_{adv}}{\partial t} + \frac{\partial[X_i]_{conv}}{\partial t} + \frac{\partial[X_i]_{loss}}{\partial t} + \frac{\partial[X_i]_{mix}}{\partial t}, \quad (1)$$

79 where $[X_i]$ is the mixing ratio of tracer i , and the tendencies correspond to vertical ad-
 80 vection (*adv*), a convective source (*conv*), parameterized chemical loss (*loss*) and mixing
 81 (*mix*).

The advective tendency for tracer i is given by the flux-form conservation equation:

$$\frac{\partial[X_i]_{adv}}{\partial t} = -\nabla \cdot (\vec{v}[X_i]) - \frac{\partial}{\partial p}(\omega[X_i]), \quad (2)$$

82 where \vec{v} is the horizontal velocity vector, p the pressure and ω the vertical velocity in
 83 pressure coordinates. Making the assumption that the horizontal distribution of tracer i
 84 is uniform, equation (2) can be written as

$$\frac{\partial [X_i]_{adv}}{\partial t} = -[X_i] \nabla \cdot \vec{v} - \frac{\partial}{\partial p} (\omega [X_i]). \quad (3)$$

85 The horizontal divergence ($\nabla \cdot \vec{v}$) is prescribed as well as the vertical velocity in pres-
 86 sure coordinates (ω). We solve the vertical part of equation (3) using the first-order
 87 finite-volume scheme of *Godunov* [1959], which is mass-conservative and positive definite.
 88 Omitting the horizontal term, a finite-volume discretization of equation (3) simply states
 89 that the rate of change of tracer mass at a given column level with pressure thickness Δp ,
 90 $\partial ([X_i] \Delta p) / \partial t$, is given by the flux of tracer mass through the upper and lower bound-
 91 aries of the cell. The flux through the upper boundary exactly equals the flux through
 92 the lower boundary of the cell above with opposite sign and the mass of the tracer is con-
 93 served in the column when using the Godunov scheme. The scheme used here is identical
 94 to the one dimensional first-order version of the *Lin and Rood* [1996] transport scheme
 95 [*Lauritzen*, 2007]. The advantage of first-order finite-volume schemes is that they are
 96 inherently positive definite but they are usually considered too diffusive for long simu-
 97 lations. In this single-column model, however, the sources and sinks for the tracers are
 98 larger than the internal numerical diffusion, hence a low order scheme can be justifiably
 99 used in this setting.

100 Having predicted the change in tracer mass due to vertical transport, we convert it to
 101 mixing ratio by dividing the tracer mass $[X_i] \Delta p$ by Δp . Hereafter we update the mixing
 102 ratio due to horizontal divergence which obviously changes the total tracer mass in the

103 column. It is noted that the discretization scheme used here preserves the mixing ratio
104 for any prescribed ω field.

105 Vertical velocities used to drive the model are (a) considered constant in time or (b)
106 vary monthly. They are derived from European Center for Medium range Weather Fore-
107 casts (ECMWF) analysis data for the years 2005 and 2006. Runs are with 2006 winds
108 except where noted. Figure 2a illustrates tropical averaged vertical velocities for four
109 seasons in 2006. The maximum tropical upwelling at all altitudes is found in December–
110 February (DJF), and the minimum from the surface to 70hPa in June–August (JJA). This
111 seasonality is expected from the seasonality of the Brewer-Dobson circulation [*Rosenlof,*
112 1995].

113 The ECMWF velocity field implicitly includes the impact of deep convection, which
114 is treated separately in the model. Hence we also conduct sensitivity experiments in
115 which the advective velocity is constrained to represent regions without deep convec-
116 tion. We do this using two methods. First, by selecting regions where the monthly
117 mean Outgoing Longwave Radiation (OLR) is greater than 240 Wm^{-2} . This value was
118 found to exclude broad regions of tropical deep convection over Africa, Indonesia, S.
119 America and the Inter-Tropical Convergence Zone (ITCZ). OLR data was taken from
120 National Oceanic and Atmospheric Administration (NOAA) Interpolated OLR for the
121 same time period as the ECMWF velocities (2006). NOAA Interpolated OLR was ob-
122 tained from the NOAA Earth System Research Laboratory, Physical Sciences Division
123 (<http://www.cdc.noaa.gov/>). The second method sorts the vertical velocities for those
124 regions where the cloud fraction (see below) is less than 0.15. This also eliminates the
125 same regions, but also varies in altitude, providing a slightly finer screen. The thick

126 gray lines in Figure 2a illustrate the effect of removing convective regions using these two
 127 methods (dark gray for cloud fraction, light gray for OLR): the clear sky advection in the
 128 troposphere changes sign and air is mostly subsiding ($\omega > 0$) up to the TTL. The effect
 129 on the model results is described in section 4.2.

130 The model is coded in pressure coordinates, with $\Delta p = 4\text{hPa}$. Vertical velocities are
 131 converted to pressure coordinates (ω). The results are not strongly sensitive to the vertical
 132 coordinate ($\Delta p = 2\text{hPa}$ yields similar results).

3.2. Mixing

Because the transport is explicitly mass conserving and strong convergence of vertical velocity exists in the TTL, we run some simulations with an optional mixing term to represent the other two dimensions of motions in the TTL. Mixing is parameterized as a relaxation to background conditions (zero source) with some characteristic time, so that

$$\frac{\partial[X_i]_{mix}}{\partial t} = -[X_i] \frac{(1 - \Delta t/\tau_{mix})}{\Delta t} \quad (4)$$

133 Where Δt is the timestep in days and τ_{mix} is in days. In the standard runs, mixing is
 134 turned off.

3.3. Convection

Convection is parameterized assuming a fractional source f and a source mixing ratio $[X_i]_{src}$ so that

$$\frac{\partial[X_i]_{conv}}{\partial t} = \alpha f \frac{([X_i]_{src} - [X_i])}{\Delta t} \quad (5)$$

135 Here α is a ‘convective efficiency’ term that reflects how long it would take for 100%
 136 cloud cover to reset the mixing ratio to the surface source. Large scale tropical convective
 137 systems have lifetimes of ~ 6 hours (as measured by the autocorrelation of mean rain rates,

138 see *Atlas et al.* [1990]), and isolated lines of forced tropical thunderstorms may last 1–2
 139 hours [*Wilson and Megenhardt*, 1997]. We assume that the larger storms may efficiently
 140 detrain and mix tracers in the TTL (and have more than enough mass flux to do so), and
 141 that smaller storms may not completely replace all the air. So we set $\alpha = 1/3$ hours⁻¹ (or
 142 a lifetime of 3 hours). $[X_i]_{src}$ is chosen to be broadly representative of average tropospheric
 143 distributions of the four tracers. Thus $[X_i]_{src}$ equals 100ppbv for CO, 600pptv for C₂H₆,
 144 50ppbv for C₂H₂ and 1pptv for ²²²Rn. It is set to 1pptv for CH₂Br₂, CHBr₃ and CH₃I.

145 This formulation can be shown to be identical to an entraining and detraining mass
 146 flux convective scheme, for example, that of *Zhang and McFarlane* [1995], used in the
 147 NCAR Community Atmosphere Model [*Collins et al.*, 2006], if we neglect downdrafts and
 148 entrainment. The fractional source f is estimated using seasonal or monthly cloud fraction
 149 derived from the CloudSat 94 GHz cloud radar [*Stephens et al.*, 2008], shown in Figure 2b.
 150 CloudSat is a cloud radar that provides radar reflectivity from thick clouds, hence it is a
 151 good proxy for convection. Since tracer transport tends to follow the humidity transported
 152 in convection, f increases where the main convective outflow level (anvil clouds) are found.

3.4. Loss

Loss of species is represented as a simple e -folding chemical lifetime τ_l where the time
 tendency of tracer $[X_i]$ at time $t+1$ is based on the average value of $[X_i]$ (including
 convection and advection) over the time step, thus

$$\frac{\partial[X_i]_{loss}}{\partial t} = -[X_i]e^{(-dt/\tau_l)} \quad (6)$$

153 Chemical loss is a function of tracer lifetime. In this work we will focus on 4 represen-
 154 tative tracers, CO, C₂H₆ (ethane), C₂H₂ (acetylene) and ²²²Rn (radon), with τ_l in days

155 of 60, 45, 15 and 4 respectively. We also examine CH_2Br_2 (dibromomethane), CHBr_3
156 (bromoform) and CH_3I (methyl iodide) with lifetimes of 120, 26 and 6 days respectively.

157 For CO , C_2H_6 , C_2H_2 and CH_2Br_2 , the atmospheric loss is due to oxidation by OH . For
158 CHBr_3 and CH_3I , photolysis is the main loss [*World Meteorological Organization*, 2007].

159 In general, the lifetime is a function of OH and/or varies with solar flux and temperature.

160 Here we have neglected these variations, which are likely not large in the TTL [*Sinnhuber*
161 *and Folkins*, 2006]. For ^{222}Rn , radioactive decay is the main loss, and does not vary.

4. Results

162 For steady state simulations, the model is run for 720 days with a time step of one hour.

163 The vertical domain is 0–40km and $\Delta p = 4\text{hPa}$. The vertical velocity (ω) at the top and

164 bottom is set to zero. ω is constant in time for steady state runs. For examination of the

165 annual cycle it varies smoothly between monthly mean values (Section 4.8). We will show

166 results from the final time step for tendencies or tracer values. With constant advection,

167 we can run the model to near equilibrium, that is $\frac{\partial[X_i]}{\partial t} = 0$. This is achieved for all but

168 the longest lived tracers (such as CH_2Br_2) after ~ 150 days. Final values are not sensitive

169 to the initial conditions. Results of runs where the vertical velocity and convection are

170 allowed to vary over time are shown in Section 4.8 to investigate how the annual cycle

171 affects the results and understand what drives the annual cycle.

4.1. Basic Results

172 Results for the ‘base’ case of the model with DJF tropical mean conditions are shown

173 in Figure 3. Profiles from 4 tracers are shown: CO , C_2H_6 , C_2H_2 and ^{222}Rn . The profiles

174 have been normalized to their maximum value. Also shown is the scaled (by 0.5) cloud
175 fraction (f).

176 In general, the longer lifetime and lack of mixing allow tracers such as CO and C₂H₆
177 to build up to near emission levels in the troposphere. Some decay is seen in C₂H₂ and
178 radon in Figure 3. Vertical advection causes the peak in tracer mixing ratio (seen clearly
179 for radon in Figure 3) to be 1–2km above the maximum convective outflow at 11km. The
180 mixing ratio peak is slightly higher for longer lived species (but less distinct). Above this
181 level, tracer concentrations tail off rapidly with height.

182 Figure 4 illustrates the tracer concentrations in the TTL. In order to construct the
183 values in Figure 4 and Table 2 for comparison to observations, annual means are used
184 from the second year of runs with an annual cycle. Quantitatively, values are similar to
185 an average of four seasonal steady state runs. Above 18km, there is very little C₂H₂ or
186 radon left, while for C₂H₆ (45 day lifetime) and CO (60 day lifetime) some tracer is lofted
187 up to 20km and higher. At 20km, 3–5% of the ‘source’ value remains for CO and C₂H₆
188 (Table 2).

189 Simulated tracer values (Table 2 and Figure 4) quantitatively compare well to those from
190 ACE (Table 1). ACE values at 20km are slightly larger. This may be due to variations
191 in vertical structure of loss, uncertainties in vertical velocity, or other sources. Observed
192 CO does not go to zero in the stratosphere (Figure 1), so there is mixing and/or chemical
193 sources, adding to the observed CO concentration (and not represented in the model).
194 ACE fractions at 18km just above the tropopause are similar to simulated values, while
195 ACE fractions at 16km are consistently smaller than the simulations, perhaps indicating
196 different efficiency to convection as a function of height. This might be due to the fact

197 that ‘overshooting’ convection (convection above its level of neutral buoyancy) will tend
198 to collapse rapidly back down and detrain at a lower level. But in general the model
199 approach can reproduce the tracer decay observed from ACE. The convective efficiency
200 (analogous to α in equation 5), could be lowered or made a function of altitude to reflect
201 ‘overshooting’. This would better reproduce the observed fraction from ACE in the upper
202 troposphere. The efficiency would be reduced at higher altitudes above the level of neutral
203 buoyancy (about 12–14km). This has not been done in the simulations.

204 The balance of terms in the model for each tracer is presented in Figure 5. Tendencies
205 represent steady state values once the model has reached equilibrium ($\frac{\partial[X_i]}{\partial t} = 0$). For CO
206 and C₂H₆, the convective source (CONV) dominates up to ~17km, 2km below the top
207 of the convective region. The convective tendency is balanced by chemical loss (LOSS)
208 and vertical advection (ADV). Advection is not important below the TTL (~200hPa)
209 where the convective source is large (see Section 4.2 below). Vertical advection begins to
210 dominate just above the cold point, with a spike as convection goes to zero. Advection is
211 more important for longer-lived species. Small amounts of convection are able to maintain
212 elevated mixing ratios several kilometers above the top of convection for longer lived
213 species.

4.2. Effect of Vertical Velocity

214 As noted in section 3.1, vertical velocities from ECMWF include convective transport.
215 This results in ‘double counting’ the convective influence. We have tested this effect in
216 several ways, but conceptually the most robust is to average the vertical velocity only
217 over those regions without convection, as shown in Figure 2a (gray lines for DJF) using
218 two methods. The vertical velocities now indicate subsidence $\omega > 0$ over a broad region

219 of the troposphere, up to the TTL for both cases. Sorting by cloud fraction is done at
220 each ECMWF level, so it is a finer grain sort than the column sort by OLR. Thus there
221 is less subsidence, particularly above the convective peak.

222 The resulting model simulations with such ω profiles are shown in Figure 6 for CO and
223 radon. Removing convective uplift has only a minor effect on the tracer mixing ratios.
224 Quantitatively the fraction of tracer remaining at any altitude is 0–3% less for the sorted
225 velocity (subsidence in the troposphere), lower for tracers with shorter lifetimes. This
226 may seem surprising, but the result is logical because advection in the troposphere where
227 subsidence occurs (below 100hPa) is not an important part of the tracer tendencies and
228 convection dominates (Figure 5). The effect of having subsidence in the troposphere
229 slightly reduces the advective tendency from 150–100hPa. If a sort by cloud fraction is
230 used, there is little change in the balance of processes in the TTL. The annual cycle is
231 not affected by a change in vertical velocity. Thus removal of convection from the vertical
232 velocities does not qualitatively affect the model solutions. The quantitative effects are
233 very small when the sort is done by cloud fraction, and preserves vertical velocities in the
234 TTL above convective regions. This is because most of the difference in ω is below the
235 level where advection dominates the tendencies.

236 However, it is clear that above the peak in tracer mixing ratios and into the lower
237 stratosphere, vertical velocities are critical for understanding tracer profiles. We explore
238 this further by varying the vertical velocity profile in the simulations, again, for two
239 tracers (Figure 7a and b for CO and radon), for two seasons (DJF and JJA). In Figure 7
240 we run six cases, with vertical velocity scaled by 0.25, 1 and 4 for DJF and JJA. Note
241 that the downward velocity at 19–20km in JJA (Figure 2a) is an effective cap on tracer

242 propagation. For CO, the spread of tracer mixing ratios at 19–25km in DJF is due to
243 vertical velocity. For radon, this is still the case (higher vertical velocities have radon
244 perhaps 1km higher than the other cases). Changes below the convective peak at 12km
245 are small in both cases.

4.3. Sensitivity

246 In this section we discuss the sensitivity of the model to various choices of parameters,
247 including mixing and chemical loss.

4.3.1. Mixing

249 Because the advection scheme in the model is strictly conservative for mixing ratio, we
250 add an optional relaxation with a variable timescale. Shorter timescales imply stronger
251 mixing. In the atmosphere, motion in the other 2 dimensions tends to effectively mix or
252 diffuse a tracer. Thus we explore adding parameterized mixing to the model (Equation 4)
253 to simulate these processes.

254 Figure 8 illustrates the effect of adding a mixing term. Runs are performed with $\tau_{mix} =$
255 60, 30, 10 (days) and no mixing, where longer times correspond to less mixing (Equa-
256 tion 4). Winds are from DJF 2006 and the model is run 720 days. Tracer concentrations
257 throughout the column are reduced. For CO (Figure 8a), a longer lived species, mixing
258 dominates the total tracer tendency when it is less than the timescale for loss. For radon
259 (Figure 8b), with a lifetime much shorter than mixing, loss still dominates since the mix-
260 ing timescale is longer, and mixing does not affect the profile as much. Thus mixing is
261 more important for longer-lived species.

4.3.2. Loss

263 We have also explored several different alternative schemes for describing the chemical
264 loss. These include changing the loss from an exponential decay to a linear ramp so that
265 $\frac{\partial[X_i]}{\partial t} = [X_i]\frac{dt}{\tau}$. Then τ becomes the loss in percent per time step (or unit time). This
266 change does not affect the solution appreciably. Changing the loss timescale by a factor
267 of 4 does affect the profiles for short lived species like radon, but is not as important for
268 longer lived tracers (such as CO). This is to be expected from the magnitude of tendency
269 terms in Figure 5.

4.4. Seasonal Tests

270 Figure 9 illustrates the impact of seasonal differences in convection and vertical motion
271 on tracer profiles. Four runs are performed with winds from each season (DJF, MAM,
272 JJA, SON) run for 720 days. In the tropical zonal average ($\pm 20^\circ$ latitude) convective
273 cloud fraction is nearly constant (Figure 2b), but does reach slightly higher altitudes in
274 DJF. This impacts the tracer concentration up to 15km. However, at 15km and above,
275 the largest effect is the difference in vertical velocity, which is higher throughout the
276 TTL in DJF (Figure 2a). For the tropical average, it is the difference in vertical velocity
277 that sets the seasonal cycle of tracer mixing ratios at the top of the TTL and in the
278 stratosphere. This is also true for shorter lived species (Figure 9b), but only below 18km
279 where significant tracer still exists. We return to this point after discussing the role of
280 convection. Note that for JJA the average vertical velocity is nearly zero at ~ 19 km
281 (Figure 2a), so tracer is not advected above 19km in a steady advection model in JJA.

4.5. Effects of Convection

282 One of the main drivers of this work is to understand how a convective source of short
283 lived tracers effects the TTL. To examine this we vary convective strength, and discuss
284 variations in the height of convection.

285 4.5.1. Convective Magnitude

286 We have also varied the strength (magnitude) of convection, by scaling the convective
287 source by a factor of 0.25, 1 and 4 in both DJF and JJA. The resulting simulations are
288 shown in Figure 10. The thin lines show the different cloud fractions, (scaled by 0.5 for
289 clarity on the plots) and the thick lines the resulting tracer profiles. Below the TTL,
290 weaker convection leads to lower mixing ratios in both seasons, and stronger convection
291 increases mixing ratios. For very strong convection, the profile is nearly locked to the
292 convective source in both cases. Above the peak mixing ratio at 14–15km however, the
293 differences due to convection in Figure 10a for CO are small. Figure 10a indicates that
294 differences in tracer mixing ratio above about 18km are mostly seasonal: that is, they
295 are due to differences in vertical velocity in the lower stratosphere, not due to convective
296 input. For short lived species such as radon, the strength of convection up to the top
297 of convection does have an impact, but in no case does significant tracer end up in the
298 stratosphere above 19km. Thus the seasonal cycle of vertical velocity is more important
299 than variations in convective magnitude above the tropopause.

300 4.5.2. Convective Top

301 Because of the model construction, advection takes air and moves it from the convective
302 region. If the vertical velocity is downward above the top of convection, this essentially
303 ‘caps’ the tracer transport. As indicated in Figure 2a, if the convective regions are removed

304 from the velocity field, then there is an effective cap at 13km (based on sorting by $f <$
305 0.15). Experiments indicate that allowing convection above this to 14km will inject some
306 tracer into the stratosphere, and allowing convection to 16km or higher will allow a similar
307 amount of tracer to reach the stratosphere as in a case with no cap on convection. Thus
308 while it is important to sort out the true clear-sky vertical motion field in the TTL, it does
309 not appear to affect tracer transport into the stratosphere as long as convection reaches at
310 least 14–16km. Note that there is clear sky radiative heating above 15km [Gettelman *et al.*,
311 2004a] in the TTL. Motion between 12–15km is complex, with subsidence and upward
312 motion forced by the distributed wave effects of convection above the main convective
313 outflow (see discussion in Fueglistaler *et al.* [2008]).

4.6. Regional Differences

314 Finally, we decompose the vertical velocity from ECMWF analyses and CloudSat re-
315 gionally and seasonally to look at variations in space as well as in time. We focus on 4 key
316 regions and seasons: (1) the JJA Asian Monsoon (5–35°N,60–120°E), the Western Pacific
317 (20°S–20°N, 100–180°E) in (2) DJF and (3) JJA and (4) the Eastern Pacific (20°S–20°N,
318 180–270°E) in DJF. These regions are important for air entering the stratosphere (1–3)
319 or notable for being capped with upper level subsidence (4). Simulations using vertical
320 velocities and convection for these four locations are illustrated in Figure 11 for CO and
321 radon. Results based on the tropical average (MEAN) are also shown in Figure 11. In
322 the regions with more convection than the tropical average (all but the Eastern Pacific),
323 profiles are similar up to the peak at 13–15km for both CO (Figure 11a) and radon (Fig-
324 ure 11b). The monsoon region in JJA has the highest CO (Figure 11a), but not the highest
325 convection (found in the Western Pacific in DJF). Significant vertical motion associated

326 with the monsoon anticyclone contributes to elevated tracer values. The Western Pacific
327 in DJF has lower vertical velocities or even negative velocities around and above the cold
328 point (noted first by *Sherwood* [2000] and *Gettelman et al.* [2000]). Thus convection and
329 vertical velocity combine to create the TTL profiles of short lived species. Convection is
330 important in the troposphere and lower TTL, and vertical velocities dominate at the cold
331 point and above.

4.7. Bromine and Iodine

332 The model can be configured to represent different tracers with different chemical loss
333 timescales. The set of tracers described above represents observed hydrocarbon tracers
334 with a range of lifetimes. We have also configured the model to represent tracers impor-
335 tant for ozone concentrations in the stratosphere and stratospheric bromine and iodine.
336 Figure 12 shows final concentrations in the TTL for a set of tracers with different lifetimes:
337 CH_2Br_2 (120 days), CHBr_3 (26 days) and CH_3I (6 days). The plot represents averages
338 from a run with an annual cycle (similar to Figure 4). As expected, there is significant
339 transport of CH_2Br_2 , and not much transport of CH_3I above convection. CHBr_3 (bromo-
340 form), is an important reservoir of potential bromine for the stratosphere. Approximately
341 28% of the surface source makes it to 18km in DJF as CHBr_3 , while $\sim 70\%$ of CH_2Br_2
342 does (Table 2).

343 Assuming boundary layer concentrations (and range) for CH_2Br_2 and CHBr_3 of 1.1pptv
344 (0.5–1.5) and 1.6pptv (0.5–2.4) [*World Meteorological Organization*, 2007], this implies
345 0.8pptv (0.35–1.1) CH_2Br_2 and 0.5 pptv (0.1–0.7) from CHBr_3 . These values are within
346 the range of CHBr_3 and CH_2Br_2 measurements reported by *Schauffler et al.* [1999], *Em-*
347 *mons et al.* [2000] and *Tuck et al.* [2004]. They are higher than results from *Laube et al.*

348 [2008], but are well within the range of uncertainty given by variable boundary layer con-
349 centrations which may vary strongly from region to region. Assuming all this bromine
350 would be released in the stratosphere, simulations imply that 2.8pptv of bromine (range
351 of 1.1–4.1 from observed concentrations) may be entering the stratosphere as CH_2Br_2 and
352 CHBr_3 .

353 As noted by *Sinnhuber and Folkins* [2006], the products of CHBr_3 oxidation can be
354 rapidly removed by condensation onto ice, so lofting CHBr_3 above regions with cirrus
355 clouds (above the cold point) is critical. The seasonal transport peaks in DJF with peak
356 mean vertical velocities (Figure 13), consistent with Figure 9. Transport of CHBr_3 is more
357 efficient in DJF due to faster vertical velocities.

4.8. Annual Cycle

358 The model can also be configured to run with time varying inputs of vertical velocity
359 and/or convective sources. This allows exploration of the annual cycle of tracers in the
360 TTL and lower stratosphere. For these simulations, the model was ‘spun up’ for 120 days,
361 and then run through a complete annual cycle using linear interpolation between monthly
362 mean inputs (velocities and convection). Results can be compared to observations, and
363 inputs can be held constant to understand which components (convection or vertical
364 velocities) contribute to the annual cycle.

365 Figure 14 illustrates concentrations (as a fraction of the source) for CO (top) and C_2H_2
366 (bottom). The BASE case at 70 hPa (solid lines) has a fairly large amplitude (0.1-0.55)
367 with a peak in the early part of the year (February), just after the peak in vertical velocity,
368 and a minimum in August (day 220), when velocities are negative in the lower stratosphere.
369 The amplitude of the annual cycle is larger for C_2H_2 (almost no tracer remains in July-

370 August), and the phase is similar (with extrema a few days earlier than CO). Also shown
371 on Figure 14 are runs with convection limited to 14km (TOPCONV14–dotted), and with
372 constant convection (CONVCONST–dashed) or constant vertical velocity (WCONST–
373 dot-dash).

374 The capping of convection significantly reduces the tracer magnitude in Figure 14. It
375 also slightly shifts the timing of the annual cycle, moving the maximum and minimum
376 at 70 hPa for CO \sim 20 days later. The minimum in boreal summer also extends further
377 into fall. At 70hPa, if convection is held constant over the year (CONVCONST) the
378 annual cycle of mixing ratio changes slightly in September-December for CO or C₂H₂
379 (Figure 14, dashed line). However if vertical velocities are kept constant (WCONST),
380 the annual cycle at 70hPa is significantly reduced (Figure 14, dot-dashed line), consistent
381 with steady-state seasonal plots (Figure 9 and 13) illustrating the importance of variations
382 in vertical velocity for stratospheric tracer concentrations (see also *Folkins et al.* [2006],
383 *Randel et al.* [2007] and *Schoeberl et al.* [2008]).

384 The situation is slightly different at 130hPa in the TTL below the tropopause (Fig-
385 ure 15). The annual cycle in the BASE case is very small for both tracers. The simulated
386 amplitude of the tropical average annual cycle is less than observed. This may be partially
387 expected since convective inputs move around spatially, but tropical averaged cloud frac-
388 tions used in the simulations are nearly constant, and CO has defined source regions. Thus
389 the model should not be expected to reproduce the total amplitude in the troposphere.
390 The annual cycle amplitude increases (from 1% to 6% for CO) if rapid mixing (τ_{mix} =10
391 days) is added (not shown). As in the lower stratosphere, capping the convective input at
392 14km (TOPCONV14) lowers the tracer mixing ratio, and increases the relative amplitude

393 of the annual cycle, but by a smaller amount (note the vertical scales are not the same
394 in Figure 14 and Figure 15). Thus there is much less impact, particularly for CO, where
395 the change in average tracer is from 98% to 92%. Note however that the annual cycle
396 of convection and the vertical velocity now contribute significantly to the annual cycle,
397 and most of the (small) annual cycle is supplied by variations in convection. Thus in any
398 one region in the TTL below the tropopause, convection would be expected to impact
399 the annual cycle of tracer distributions, even for tracers such as CO with lifetimes of 2
400 months.

401 We can compare the seasonal cycle of CO to that observed from satellites, for example
402 the Microwave Limb Sounder on the EOS Aura platform [*Schoeberl et al.*, 2006]. At
403 146 hPa, the observed seasonal cycle of CO is about 20ppbv (or about 15% of the value
404 at 146hPa). In the model, there is almost no seasonal cycle. The tropospheric cycle is
405 likely due to variations in emissions and convective mass fluxes. However, at 70hPa, the
406 seasonal cycle amplitude is about 12 ppbv, or 10% of the tropospheric source. The model
407 has a large (40% of the tropospheric value) annual cycle at 70hPa. The annual cycle is
408 likely larger than observed due to lack of a stratospheric background CO and mixing with
409 such air. The timing of the CO seasonal cycle does agree with observations in the lower
410 stratosphere. The minimum observed CO August–October, and the peak is in January.
411 Thus the 1D model is able to produce the seasonal cycle of CO in the lower stratosphere
412 with no variation in emissions source, and also mostly with no variation in convection
413 (Figure 14).

5. Conclusions

414 This simple 1D model allows some interesting insights into TTL transport.

415 1. The 1D model can qualitatively and quantitatively reproduce the distribution of
416 short lived species in the TTL using simple transport, convective source and parameterized
417 loss. There are some differences in the slope of evanescent tracer mixing ratios between
418 observations and simulations. The model is also able to generate the right phase of the
419 annual cycle of CO, though it is quantitatively different than satellite observations in
420 the upper troposphere and lower stratosphere due to constant simulated emissions and
421 simplified transport.

422 2. Convection is important up to the tropopause, and slightly above. There is little
423 influence of velocities below the TTL (150–200hPa) on the simulated tracer concentration
424 in the lower stratosphere. Even for relatively long lived species like CO, a little convec-
425 tion contributes substantially to concentrations. However, large scale vertical advection,
426 though velocities are low, rapidly dominates above 15–17km, though some convection goes
427 up to 19km.

428 3. The bifurcation point for significant transport into the stratosphere seems to be at a
429 lifetime of 25–30 days, right around the lifetime of bromoform (CHBr_3). This is consistent
430 with trajectory based estimates of a TTL transit time of 60 days or so [*Fueglistaler et al.*,
431 2004] and a convective turnover time at 14km of 2–3 months [*Gettelman et al.*, 2002b].
432 The fraction of tracer remaining at an altitude is a function of its lifetime. This is clearly
433 seen in Figures 3 and 12, and quantitatively in Table 2.

434 4. Results allow further estimation of the transport of Very Short Lived Substances
435 (VSLS) into the stratosphere. 70% of the surface concentration of CH_2Br_2 is found at
436 18km, while 52% of CO and 28% of CHBr_3 is. This implies that ~ 2.8 (1.1–4.1) pptv of

437 additional bromine may be entering the stratosphere as CH_2Br_2 and CHBr_3 , just over one
438 half of the estimate of bromine from VLSL by *Dorf et al.* [2008].

439 5. Vertical velocity dominates tracer concentrations above the tropopause for tracers
440 with lifetimes longer than a week (C_2H_2 and longer lived species). This is clearly seen
441 in both the steady state runs in different seasons, and in the runs over an annual cycle.
442 Thus the seasonal cycle in CO above the tropopause in the lower stratosphere is due to the
443 variation in vertical velocity in the lower stratosphere, not due to variations in the input
444 concentration. With no variation in input concentration, the model is roughly able to
445 produce the seasonality (phase) of CO in the lower stratosphere. This occurs even without
446 variations in convective source, or in tropospheric emissions. Addition of a stratospheric
447 background and a variable tropospheric emission (and loss) would improve agreement in
448 the magnitude of the annual cycle in the upper troposphere. Vertical velocities below the
449 TTL do not affect tracer concentrations in the TTL as long as some convection reaches
450 a region in which clear sky velocities are upwards ($\sim 15\text{km}$ for radiative heating, possibly
451 as low as 12km for convective wave forcing).

452 How would water vapor be placed in the context of this model? To the extent that water
453 is a short lived tracer in rapid vertical motion, convection should significantly impact the
454 distribution of humidity, and it does. However, the process of condensation of water
455 differs from chemical loss, as it is (a) reversible through evaporation and (b) strongly
456 thermodynamically forced.

457 While the simulations are in reasonable agreement with observations, there are still
458 large uncertainties due to variability of short lived tracer fields. The model could be
459 developed further to fit observations by (a) adding a stratospheric source for CO and

460 variable surface emissions ($[X_{CO}]_{src}$), (b) adjusting the convective efficiency (α) and (c)
461 making chemical loss a function of altitude by relating it to OH concentrations and/or
462 solar photolysis. Nonetheless, there are limitations of a 1-D model that limit the utility
463 of further fitting to observations. For example, separating the vertical motion field into
464 convective and non-convective components for a complete diagnosis of vertical motion
465 below the level of zero radiative heating at 15km is a complex task. It is highly desirable
466 to check these estimates and conclusions against further observations, and against full 3-D
467 chemical transport models and/or coupled chemistry-climate models.

6. Acknowledgments

468 The National Center for Atmospheric Research is sponsored by the United States Na-
469 tional Science Foundation.

References

- 470 Atlas, D., D. Rosenfeld, and D. A. Short, The estimation of convective rainfall by area
471 integrals 1. The theoretical and empirical basis, *J. Geophys. Res.*, *95*(D3), 2153–2160,
472 1990.
- 473 Bernath, P. F., et al., Atmospheric chemistry experiment (ACE): Mission overview, *Geo-*
474 *phys. Res. Lett.*, *32*(L15S01), doi:10.1029/2005GL022386, 2005.
- 475 Collins, W. D., et al., The formulation and atmospheric simulation of the Community
476 Atmosphere Model: CAM3, *J. Clim.*, *19*(11), 2122–2161, 2006.
- 477 Dorf, M., A. Butz, C. Camy-Peyret, M. P. Chipperfield, K. Kritten, and K. Pfeilsticker,
478 Bromine in the tropical troposphere and stratosphere as derived from balloon-borne
479 BrO observations, *Atmos. Chem. Phys.*, *8*, 7265–7271, 2008.

- 480 Emmons, L. K., D. A. Hauglustaine, J. F. Müller, M. A. Carroll, G. P. Brasseur, D. Brun-
481 ner, J. Staehlin, V. Thouret, and A. Marengo, Data composites of airborne observations
482 of tropospheric ozone and its precursors, *J. Geophys. Res.*, *105*, 20,497–20,536, 2000.
- 483 Folkins, I., and R. V. Martin, The vertical structure of tropical convection and its impact
484 on the budgets of water vapor and ozone, *J. Atmos. Sci.*, *62*, 1560–1573, 2005.
- 485 Folkins, I., P. Bernath, C. Boone, G. Lesins, N. Livesey, A. M. Thompson, K. Walker, and
486 J. C. Witte, Seasonal cycles of O_3 , CO , and convective outflow at the tropical tropopause,
487 *Geophys. Res. Lett.*, *33*(L16802), doi:10.1029/2006GL026602, 2006.
- 488 Fueglistaler, S., and P. H. Haynes, Control of interannual and longer-term variability of
489 stratospheric water vapor, *J. Geophys. Res.*, *110*(D08107), doi:10.1029/2005JD006019,
490 2005.
- 491 Fueglistaler, S., H. Wernli, and T. Peter, Tropical troposphere-to-stratosphere trans-
492 port inferred from trajectory calculations, *J. Geophys. Res.*, *109*(D03108), doi:
493 10.1029/2003JD004069, 2004.
- 494 Fueglistaler, S., A. E. Dessler, T. J. Dunkerton, I. Folkins, Q. Fu, and P. W. Mote, The
495 tropical tropopause layer, *Rev. Geophys.*, 2008.
- 496 Gettelman, A., and T. Birner, Insights on tropical tropopause layer processes using global
497 models, *J. Geophys. Res.*, *112*(D23104), doi:10.1029/2007JD008945, 2007.
- 498 Gettelman, A., A. R. Douglass, and J. R. Holton, Simulations of water vapor in the upper
499 troposphere and lower stratosphere, *J. Geophys. Res.*, *105*, 9003–9023, 2000.
- 500 Gettelman, A., W. J. Randel, F. Wu, and S. T. Massie, Transport of water vapor in
501 the tropical tropopause layer, *Geophys. Res. Lett.*, *29*(1), doi:10.1029/2001GL013818,
502 2002a.

- 503 Gettelman, A., M. L. Salby, and F. Sassi, The distribution and influence of convection in
504 the tropical tropopause region, *J. Geophys. Res.*, *107*(D10), doi:10.1029/2001JD001048,
505 2002b.
- 506 Gettelman, A., P. M. F. Forster, M. Fujiwara, Q. Fu, H. Vomel, L. K. Gohar, C. Johanson,
507 and M. Ammeraman, The radiation balance of the tropical tropopause layer, *J. Geophys.*
508 *Res.*, *109*, doi:10.1029/2003JD004190, 2004a.
- 509 Gettelman, A., D. E. Kinnison, T. J. Dunkerton, and G. P. Brasseur, The impact of
510 monsoon circulations on the upper troposphere and lower stratosphere, *J. Geophys.*
511 *Res.*, *109*, doi:10.1029/2004JD004878, 2004b.
- 512 Godunov, S., A difference scheme for numerical computation of discontinuous solutions
513 of equations in fluid dynamics, *Math. Sb.*, *47*, 271, also: Cornell Aero. Lab. translation,
514 1959.
- 515 Holton, J. R., and A. Gettelman, Horizontal transport and dehydration in the strato-
516 sphere, *Geophys. Res. Lett.*, *28*(14), 2799–2802, 2001.
- 517 Laube, J. C., A. Engel, H. Bönish, T. Möbius, D. R. Worton, W. T. Sturges, K. Grunow,
518 and U. Schmidt, Contribution of very short-lived organic substances to stratospheric
519 chlorine and bromine in the tropics – a case study, *Atmos. Chem. Phys.*, *8*, 7325–7334,
520 2008.
- 521 Lauritzen, P. H., A stability analysis of finite-volume advection schemes permitting long
522 time steps, *Mon. Weather Rev.*, *135*(7), 2658–2673, 2007.
- 523 Lin, S. J., and R. B. Rood, Multidimensional flux-form semi-lagrangian transport schemes,
524 *Mon. Weather Rev.*, *124*(9), 2046–2070, 1996.

- 525 Park, M., W. J. Randel, L. K. Emmons, P. F. Bernath, K. A. Walker, and C. D. Boone,
526 Chemical isolation of the asian monsoon anticyclone observed in atmospheric chemistry
527 experiment (ace-fts) data, *Atmos. Chem. Phys.*, *8*, 757–764, 2008.
- 528 Randel, W. J., M. Park, F. Wu, and N. Livesey, A large annual cycle in ozone above
529 the tropical tropopause linked to the brewer-dobson circulation, *J. Atmos. Sci.*, *64*(12),
530 4479–4488, 2007.
- 531 Read, W. G., D. L. Wu, J. W. Waters, and H. C. Pumphrey, Dehydraron in the tropical
532 tropopause layer: Implications from the UARS Microwave Limb Sounder, *J. Geophys.*
533 *Res.*, *109*(D06110), doi:10.1029/2003JD004056, 2004.
- 534 Read, W. G., M. J. Schwartz, A. Lambert, H. Su, N. J. Livesey, W. H. Daffer, and C. D.
535 Boone, The roles of convection, extratropical mixing, and in-situ freeze-drying in the
536 tropical tropopause layer, *Atmos. Chem. Phys.*, *8*, 6051–6067, 2008.
- 537 Rosenlof, K. H., Seasonal cycle of the residual mean meridional circulation in the strato-
538 sphere, *J. Geophys. Res.*, *100*(D3), 5173–5191, 1995.
- 539 Salawitch, R. J., D. K. Weisenstein, L. J. Kovalenko, C. E. Sioris, P. O. Wennberg,
540 K. Chance, M. K. W. Ko, and C. A. McLinden, Sensitivity of ozone to bromine in the
541 lower stratosphere, *Geophys. Res. Lett.*, *32*, 5811–+, doi:10.1029/2004GL021504, 2005.
- 542 Schauffler, S. M., E. L. Atlas, F. Flocke, J. M. R. A. Lueb Lee-Taylor, V. Stroud, and
543 W. Travnicek, Distributions of brominated organic compounds in the troposphere and
544 lower stratosphere, *J. Geophys. Res.*, *104*(D17), 21,513–215,335, 1999.
- 545 Schoeberl, M. R., B. N. Duncan, A. R. Douglass, J. Waters, N. Livesey, W. Read, and
546 M. Filipiak, The carbon monoxide tape recorder, *Geophys. Res. Lett.*, *33*(L12711), doi:
547 10.1029/2006GL026178, 2006.

- 548 Schoeberl, M. R., et al., QBO and annual cycle variations in tropical lower stratosphere
549 trace gases from HALOE and aura MLS observations, *J. Geophys. Res.*, 113(D05301),
550 doi:10.1029/2007JD008678, 2008.
- 551 Sherwood, S. C., A stratospheric “drain” over the maritime continent, *Geophys. Res.*
552 *Lett.*, 27(5), 677–680, 2000.
- 553 Sherwood, S. C., and A. E. Dessler, A model for transport across the tropical tropopause,
554 *J. Atmos. Sci.*, 58, 765–779, 2001.
- 555 Sinnhuber, B. M., and I. Folkins, Estimating the contribution of bromoform to strato-
556 spheric bromine and its relation to dehydration in the tropical tropopause layer, *Atmos.*
557 *Chem. Phys.*, 6, 4755–4761, 2006.
- 558 Stephens, G. L., et al., Cloudsat mission: Performance and early science after the first
559 year of operation, *J. Geophys. Res.*, 113(D00A18), doi:10.1029/2008JD009951, 2008.
- 560 Tuck, A. F., S. J. Hovde, K. K. Kelly, et al., Horizontal variability 1–2km below the
561 tropical tropopause, *J. Geophys. Res.*, 109(D05310), doi:10.1029/2003JD003942, 2004.
- 562 Wilson, J. W., and D. L. Megenhardt, Thunderstorm initiation, organization and lifetime
563 associated with florida boundary layer convergence lines, *Mon. Weather Rev.*, 125(7),
564 1507–1525, 1997.
- 565 World Meteorological Organization, *Scientific Assessment of Ozone Depletion: 2006*,
566 WMO Report 50, World Meteorological Organization, Geneva, 2007.
- 567 Zhang, G. J., and N. A. McFarlane, Sensitivity of climate simulations to the parameteri-
568 zation of cumulus convection in the Canadian Climate Center general circulation model,
569 *Atmos. Ocean*, 33(407–446), 1995.

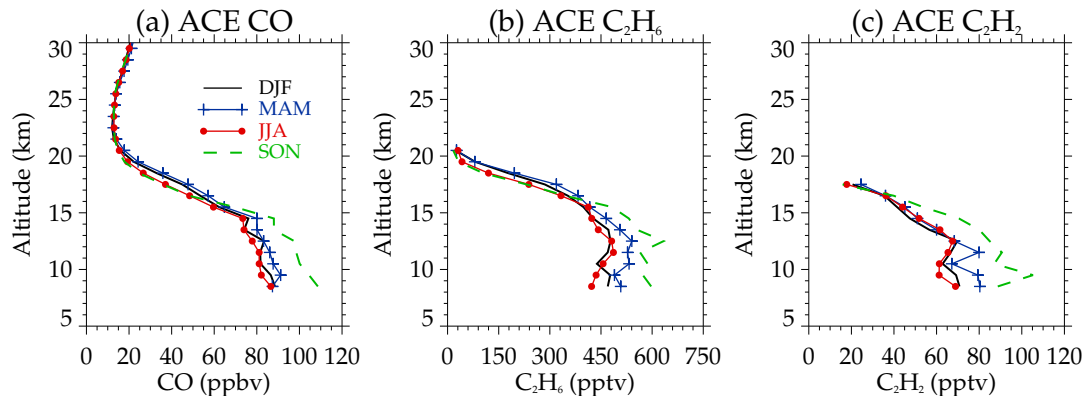


Figure 1. ACE tropical (20°S – 20°N) average mixing ratios for 2004–2006 by season for (A) CO, (B) C_2H_6 , (C) C_2H_2 .

Table 1. Percent of surface source remaining at given altitudes for tracers with different lifetimes (December–February) based on ACE-FTS observations.

Tracer	Lifetime	Percent Remaining		
		16km/100hPa	18km/79hPa	20km/58hPa
CO	60	75	50	25
C_2H_6	45	67	42	12
C_2H_2	15	57	29	4

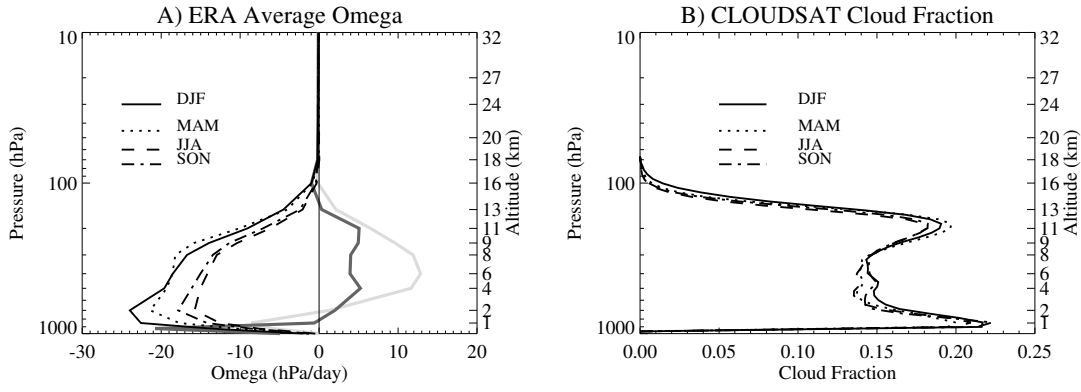


Figure 2. Tropical averaged (20°S – 20°N) seasonal profiles used as input for the simulations. A) Omega (pressure vertical velocity) from ECMWF analysis. B) CloudSat cloud fraction. Light Gray line in A is DJF omega calculated only for regions where the Outgoing Longwave Radiation (OLR) is greater than 240Wm^{-2} as described in the text. Dark Gray line in A is DJF omega sorted by regions where the CloudSat cloud fraction is less than 0.15.

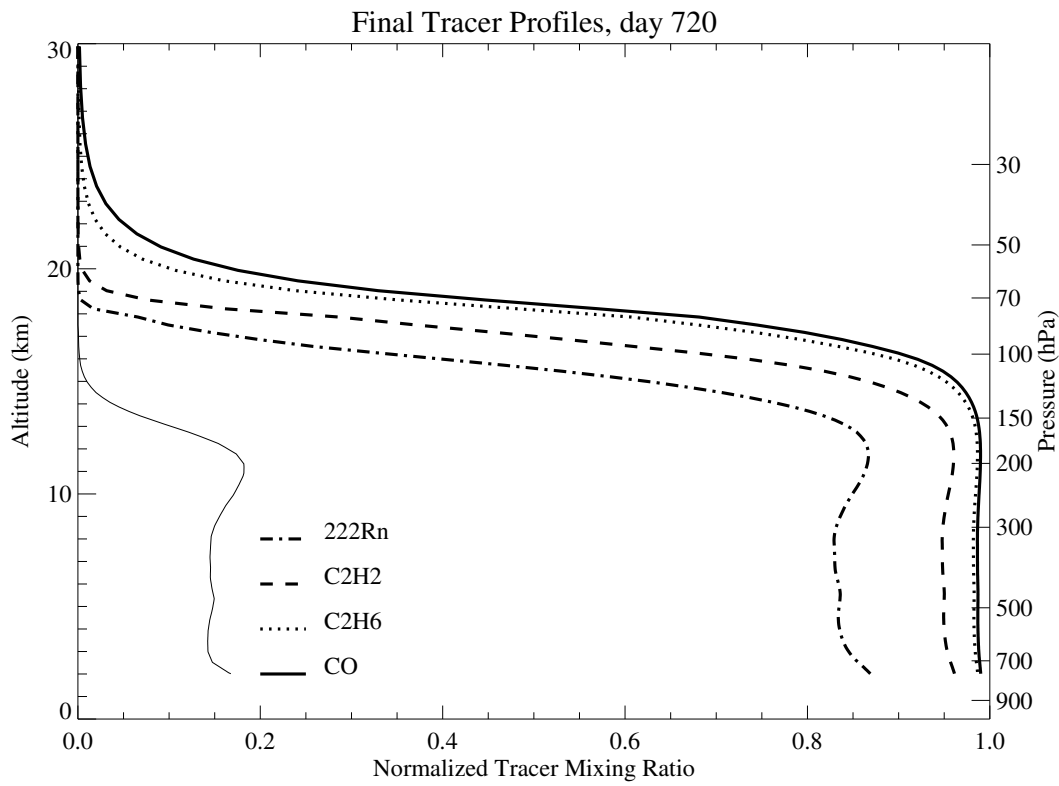


Figure 3. Final time normalized mixing ratios of CO (solid), C₂H₆ (dotted), C₂H₂ (dashed) and radon (²²²Rn: dot-dash) using DJF 2006 winds. Thin line is the cloud fraction profile (f) scaled by 0.5 for clarity.

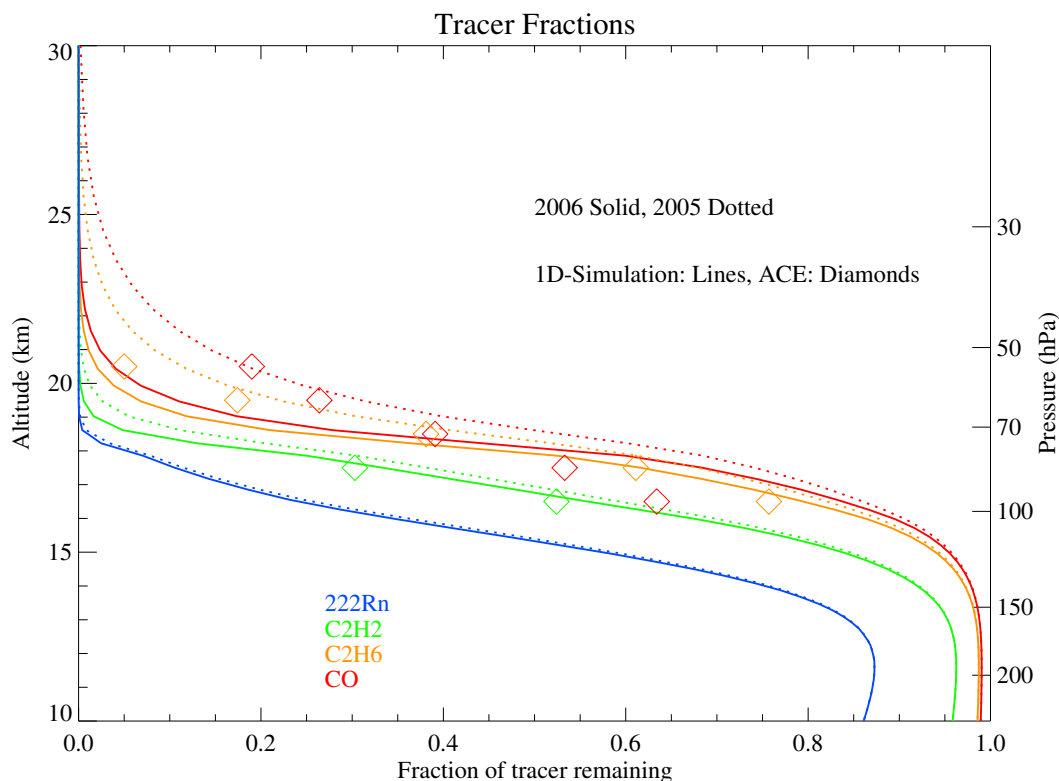


Figure 4. Annual mean normalized mixing ratios of CO (red), C₂H₆ (orange), C₂H₂ (green) and radon (²²²Rn: blue) in the TTL. Solid lines represent runs with 2006 winds, dotted lines 2005 winds. ACE observations (normalized) shown as diamonds.

Table 2. Percent of surface source remaining at given altitudes for tracers with different lifetimes based on annual averages of a model simulation with an annual cycle.

Tracer	Lifetime	Percent Remaining		
		16km/100hPa	18km/79hPa	20km/58hPa
CH ₂ Br ₂	120	93	70	18
CO	60	87	52	5.3
C ₂ H ₆	45	83	43	2.8
CHBr ₃	26	74	28	0.6
C ₂ H ₂	15	61	16	0.1
CH ₃ I	6	37	5.7	<0.1
²²² Rn	4	28	3.6	<0.1

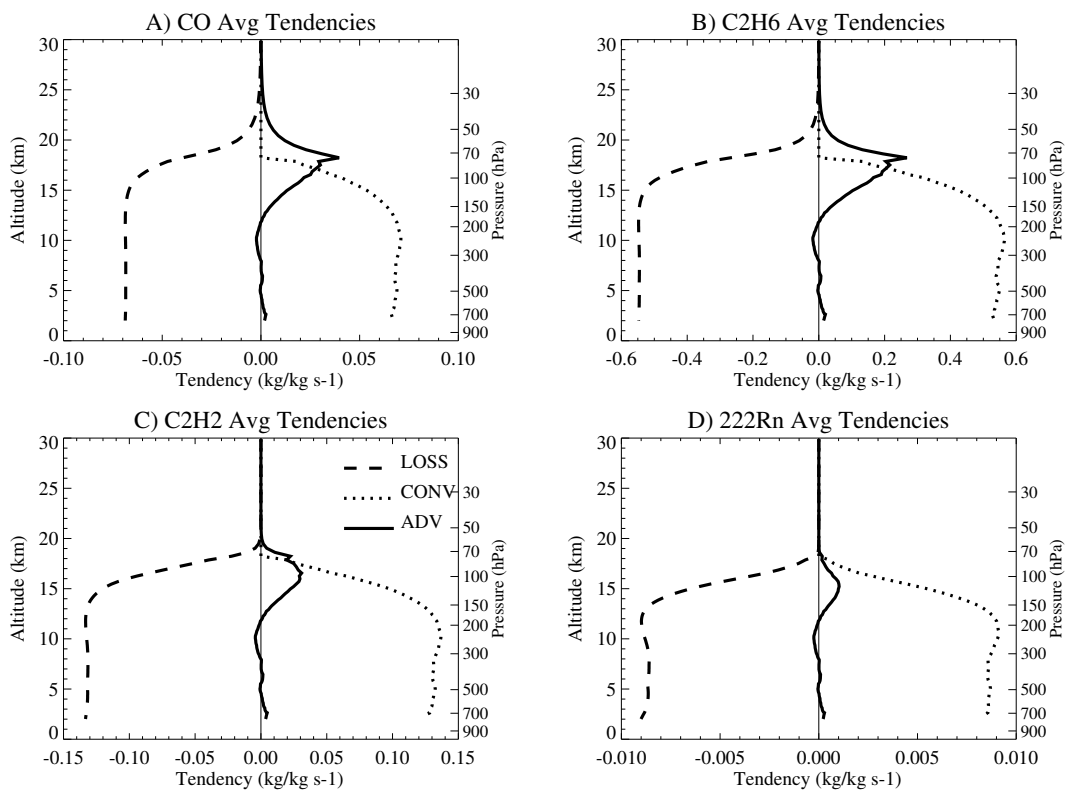


Figure 5. Final time tendencies of (A) CO (B) C₂H₂ (C) C₂H₆ (D) radon (²²²Rn). Tendencies due to Advection (ADV) solid, Convection (CONV) dotted, Loss (LOSS) dashed.

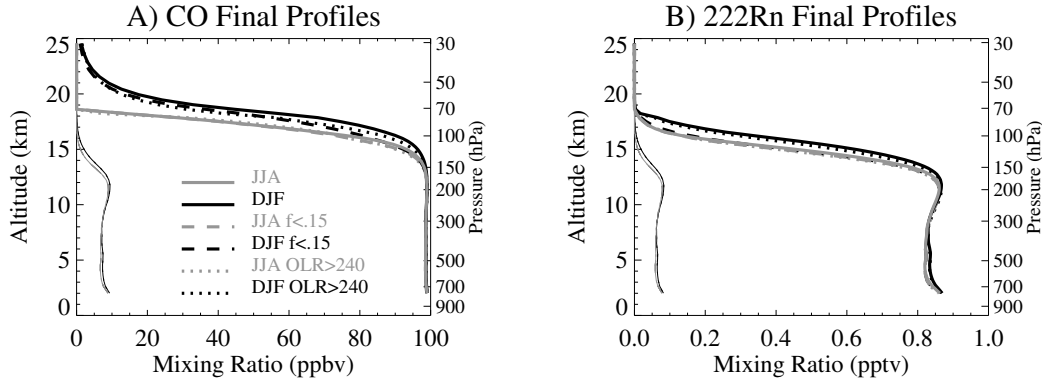


Figure 6. Final mixing ratio profiles of (A) CO and (B) Radon (^{222}Rn) for DJF (black) and JJA (gray) for the standard case (solid), with vertical velocity (ω) averaged from regions where $\text{OLR} > 240 \text{ WM}^{-2}$ (dotted) and using ω sorted by cloud fraction where $f < 0.15$ (dashed). Cloud fraction (thin lines) scaled by 50 (A) and 0.5 (B) for clarity.

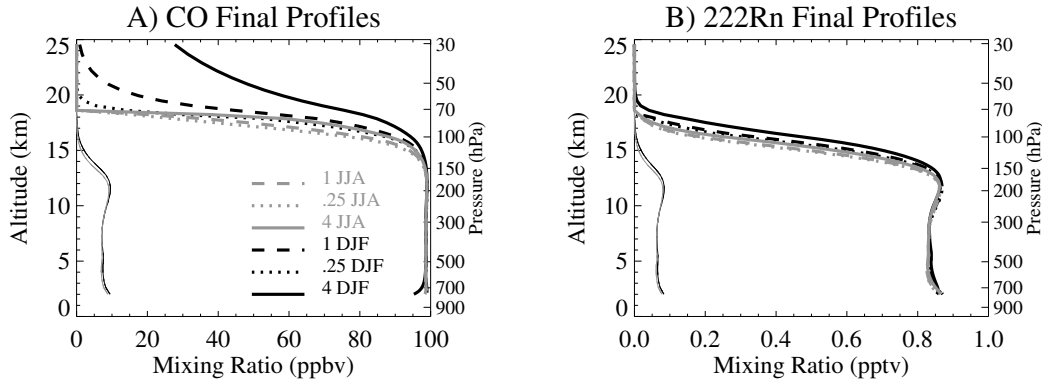


Figure 7. Final mixing ratio profiles of (A) CO and (B) Radon (^{222}Rn) with different vertical velocities (ω scaled by 0.25, 1 and 4) for each of 2 seasons (DJF, JJA). Cloud fraction (thin lines) scaled by 50 (A) and 0.5 (B) for clarity.

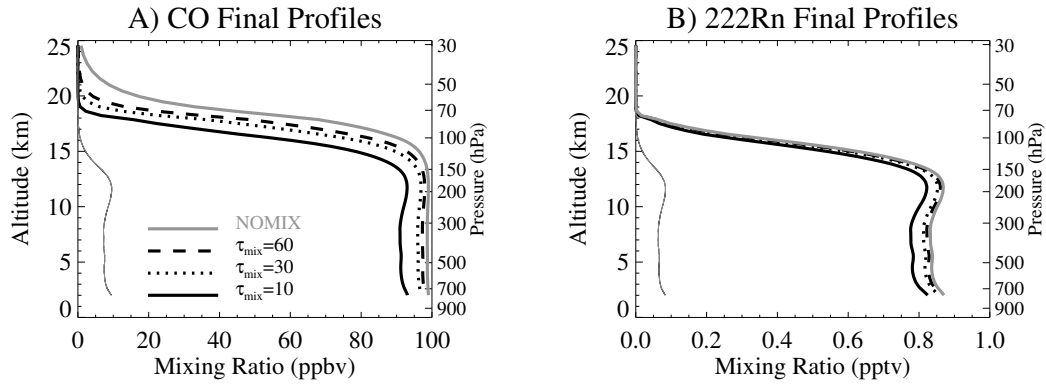


Figure 8. Final mixing ratio profiles of (A) CO and (B) Radon (^{222}Rn) for different mixing assumptions using DJF 2006 winds. Mixing is set off (NOMIX) and with timescales of $\tau_{mix}=10$, 30 and 60 days. Cloud fraction (thin lines) scaled by 50 (A) and 0.5 (B) for clarity.

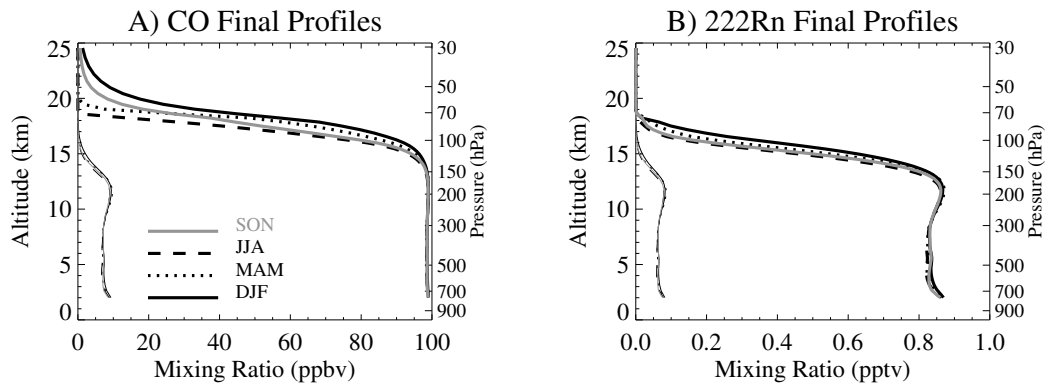


Figure 9. Final mixing ratio profiles of (A) CO and (B) radon (^{222}Rn) for DJF, MAM, JJA, SON using 2006 winds. Cloud fraction (thin lines) scaled by 50 (A) and 0.5 (B) for clarity.

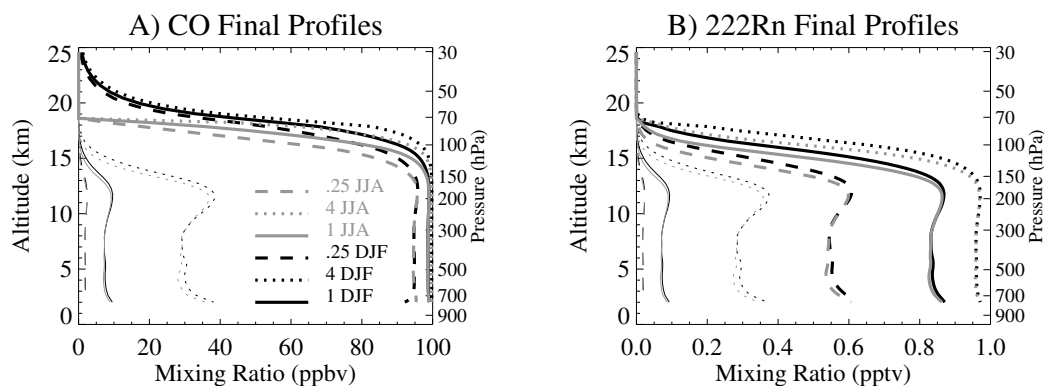


Figure 10. Final mixing ratio profiles of (A) CO and (B) Radon (^{222}Rn) for convection with different magnitudes (f scaled by 0.25, 1 and 4) for each of 2 seasons (DJF, JJA). Cloud fraction (thin lines) scaled by 50 (A) and 0.5 (B) for clarity.

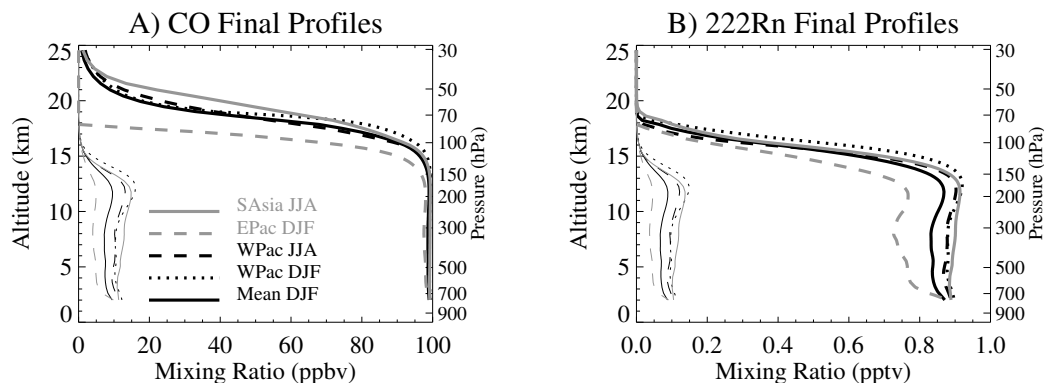


Figure 11. Final mixing ratio profiles of (A) CO and (B) Radon (^{222}Rn) for different regions. SAsia ($5\text{--}35^\circ\text{N}$, $60\text{--}120^\circ\text{E}$) in JJA, WPac DJF ($20^\circ\text{S}\text{--}20^\circ\text{N}$, $100\text{--}180^\circ\text{E}$), WPac in JJA, EPac ($20^\circ\text{S}\text{--}20^\circ\text{N}$, $180\text{--}270^\circ\text{E}$) in DJF and the tropical MEAN. Cloud fraction (thin lines) scaled by 50 (A) and 0.5 (B) for clarity.

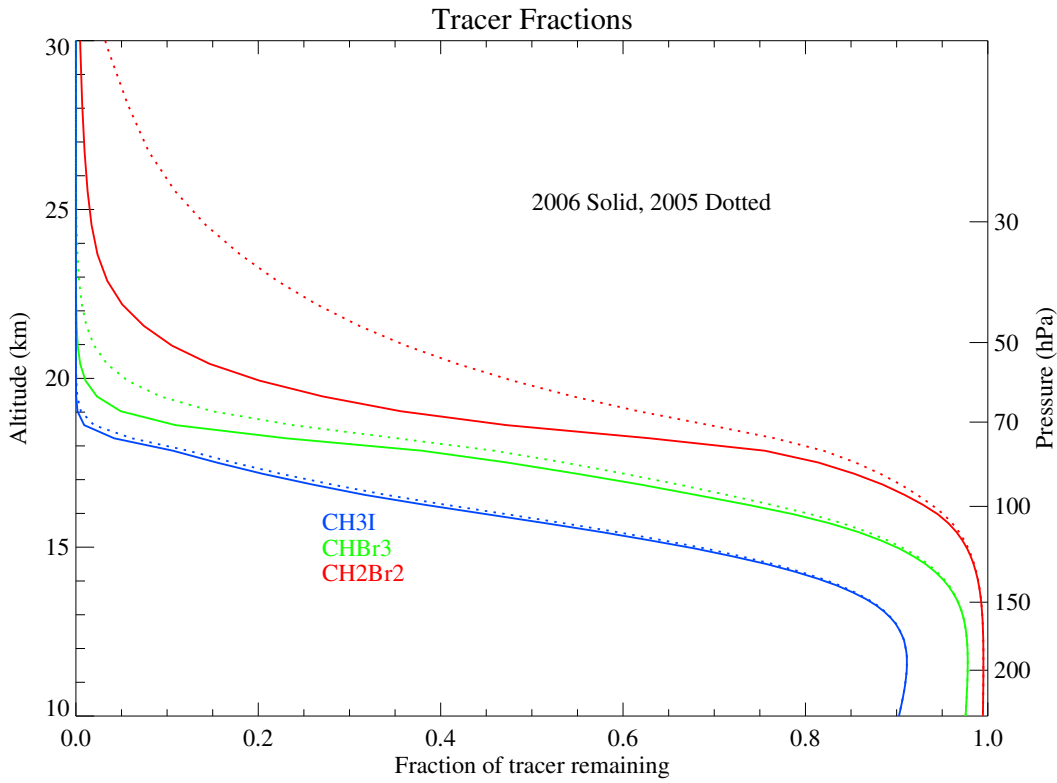


Figure 12. Average normalized mixing ratios of CH₂Br₂ (red), CHBr₃ (green) and CH₃I (blue). Solid lines represent runs with 2006 winds, dotted lines 2005 winds.

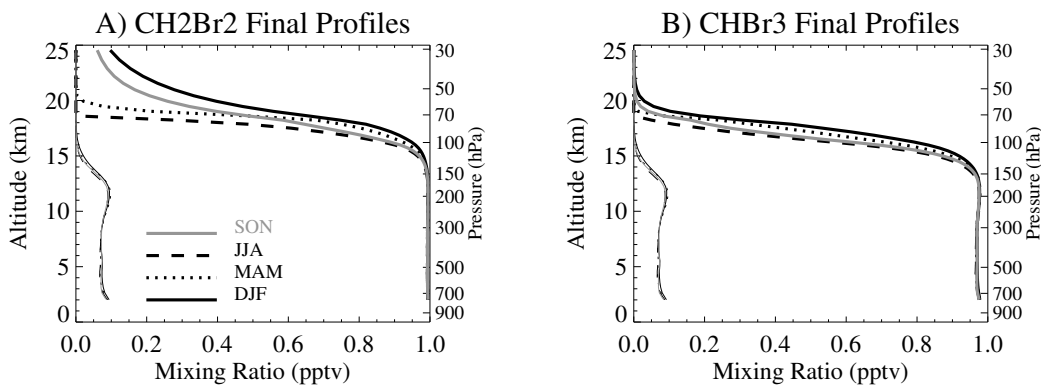


Figure 13. Final mixing ratio profiles of (A) CH₂Br₂ and (B) CHBr₃ for DJF, MAM, JJA, SON. Cloud fraction (thin lines) scaled by 50 (A) and 0.5 (B) for clarity.

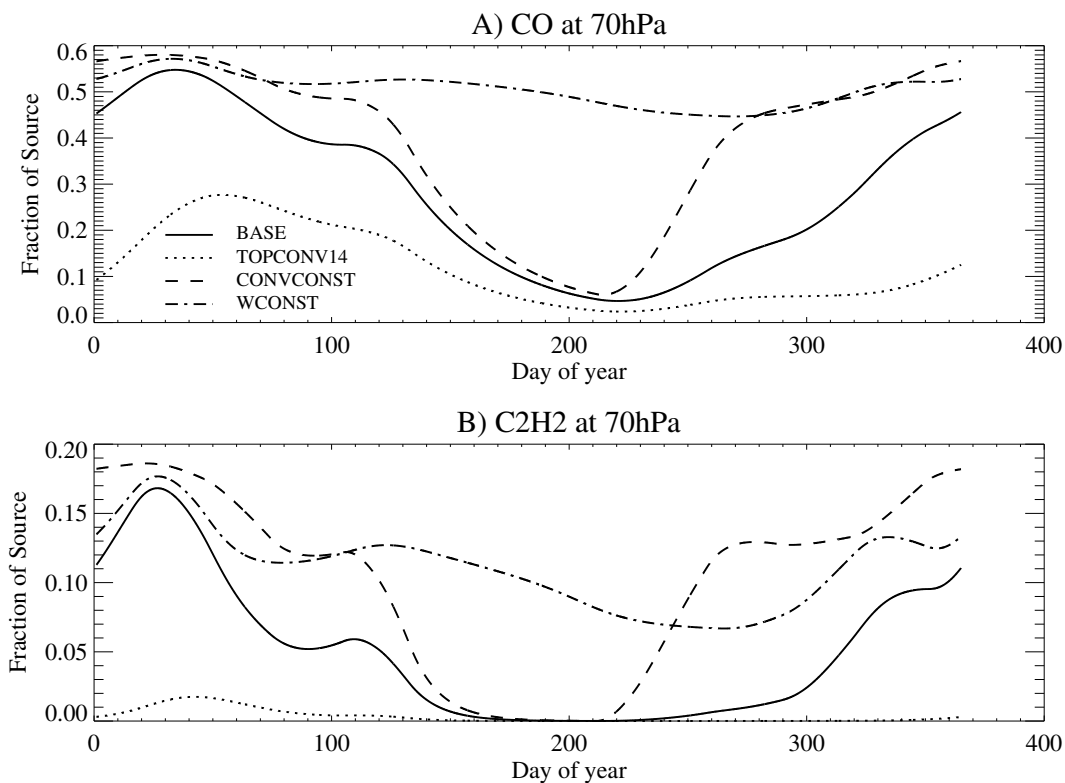


Figure 14. Normalized tracer mixing ratios as a function of time for A) CO and B) C_2H_2 at 70 hPa in a run with varying velocity and convection. Lines illustrate the BASE run (solid), a run with convection only up to 14km (TOPCONV14-dotted), convection constant in time (CONVCONST-dashed) and vertical velocities constant in time (WCONST-dot dashed).

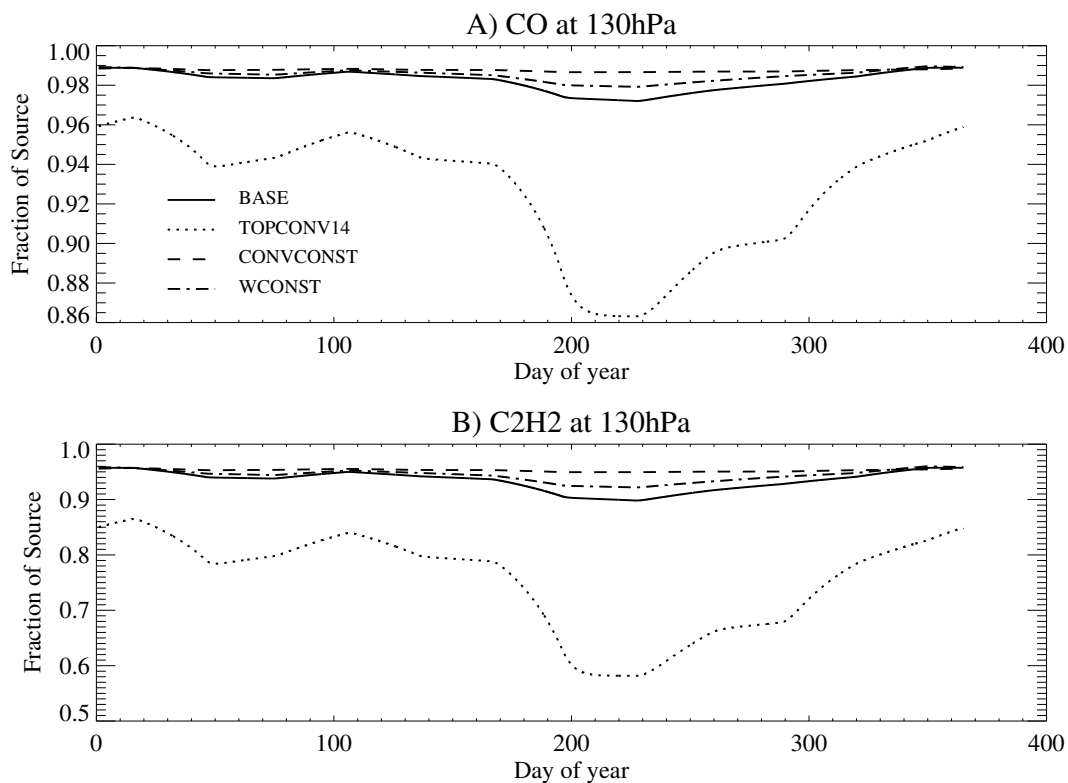


Figure 15. As for Figure 14 but for 130hPa.